

Original Research Article

A Mechanistic Formation of Phenolic and Furan-Based Molecular Products from Pyrolysis of Model Biomass Components

Samuel K. Kirkok, Joshua K. Kibet*, Thomas K. Kinyanjui, Francis I. Okanga

Department of Chemistry, Egerton University, P.O Box 536-20115, Egerton, Kenya

ARTICLE INFO

Article history

Submitted: 2022-10-25

Revised: 2022-11-16

Accepted: 2022-12-04

Available online: 2022-12-21

Manuscript ID: PCBR-2210-1235

DOI: 10.22034/pcbr.2022.367054.1235

KEYWORDS

Phenol;

Furans;

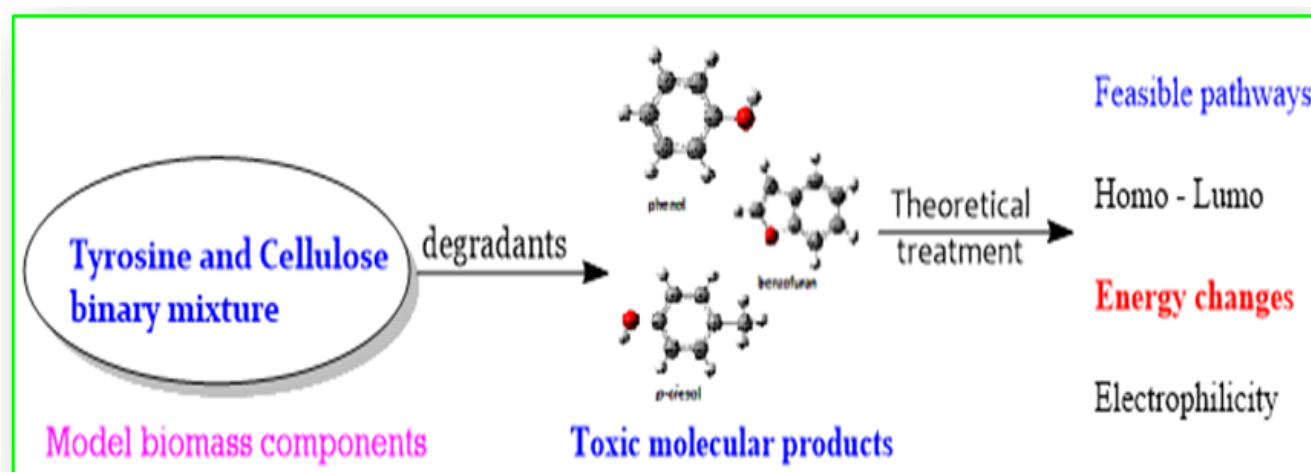
Chemical Potential;

Density Functional Theory

ABSTRACT

Herein, we critically present theoretical modeling of toxic molecular compounds from biomass pyrolysis using the density functional theory formalism at the B3LYP level of theory coupled to 3-21G basis set. Detailed molecular modeling – geometry optimization, global hardness, and chemical potentials of the selected phenols and furans are reported. The thermal energy changes and reactivity are estimated from Gaussian'09 and Chemission computational platforms. The formation of phenol and cresols are attributed to the thermally induced fragmentation of tyrosine via the rupture of the C-C bond (β -fission) which occurs via an endothermicity of +231.58 kJ/mol. The decarboxylation of tyrosine proceeds exothermally following an energy release of -14.36 kJ/mol. Subsequently, furans were formed from radical recombination during the thermal fragmentation of monomeric cellulose and tyrosine. The mechanistic formation of toxic molecular species from the thermal degradation of representative biomass materials has been proposed. From the global hardness data, it was noted that p-cresol was more reactive compared to phenol whereas alkylated benzofurans were more reactive than benzofuran because of their lower HOMO-LUMO energy gaps.

GRAPHICAL ABSTRACT



* Corresponding author: Joshua K. Kibet

✉ E-mail: jkibet@egerton.ac.ke

© 2022 by SPC (Sami Publishing Company)



1- Introduction

The mechanistic formation of reaction products from the thermal degradation of model biomass components has lately received enormous scientific research because of the importance attached to the combustion events that result in environmental pollution. It is therefore essential to explore feasible mechanistic pathways from which toxic and environmentally potent molecular products are formed from the co-pyrolysis of model biomass components such as tyrosine and cellulose. Of interest is the formation of toxic intermediate fragments under the pyrolytic regimes. For instance, tyrosine thermally degrades to *p*-hydroxy phenyl radical associated with oxidative stress in humans [1]. The current study explicitly explores mechanistic pathways for the formation of phenols and furans from co-pyrolysis of equimassic binary mixture of cellulose and tyrosine using the density functional theory (DFT) formalism at the B3LYP quantum level [2, 3].

Theoretical approaches have largely been relied upon to predict the chemical reactivity of molecules [4] using DFT calculations and the other computational methods such as Chemissian. The density functional theory has been widely used to predict reaction energies, site-reactivity, and global reactivity descriptors of the chemical systems and other varied chemical properties of molecules [2] on the basis of the Hohenberg-Kohn theorems [5]. For a given atom or molecule, the ground state energy calculation in DFT relies on electron density $\rho(\mathbf{r})$. The expression connecting energy to the electron density is given by Equation 1.

$$E(\rho) = F(\rho) + \int v(\mathbf{r}) \rho(\mathbf{r}) d\mathbf{r} \quad (1)$$

Where, $F(\rho)$ represents universal Hohenberg-Kohn function, $v(\mathbf{r})$ is the external electrostatic potential felt by an electron at a distance \mathbf{r} due to the nuclei, and E is the electronic energy. If we take the first partial derivative of Equation 1 with

respect to the number of electrons N at constant $v(\mathbf{r})$, we obtain the chemical potential (μ). This global reactivity descriptor is defined by Equation 2.

$$\mu = \left(\frac{\partial E}{\partial N} \right)_{v(\mathbf{r})} \quad (2)$$

Similarly, the second partial derivative of Equation 1 with respect to N at constant $v(\mathbf{r})$ gives the global hardness (η), as expressed by Equation 3.

$$\eta = \left(\frac{\partial^2 E}{\partial^2 N} \right)_{v(\mathbf{r})} \quad (3)$$

These global reactivity parameters can also be obtained from frontier orbitals. In this work, the global quantities which include the chemical potential, global hardness, and global softness which by definition is the inverse of global hardness was determined for the molecular products considered in this study viz phenol, cresols, benzofuran, and alkylated versions of benzofuran.

The density functional theory is employed to determine the thermal energies, frontier molecular orbitals, and electron density maps. Furthermore, the global reactivity descriptors were determined based on HOMO - LUMO energy difference. In addition, the electrostatic potentials were mapped onto electron density maps with the aim of establishing the positive or negative electrostatic potentials of the molecules under study. Biomass pyrolysis present enormous economic benefits such as pyrosynthesis of essential oils and medicinal drugs, and the biofuels production, but the negative toxic effects of the molecular products to humans and the environment health are of grave health concern. The understanding of the mechanistic formation of furans and phenols from biomass degradation are indispensable in the development of appropriate remedial strategies in the environment.

1-1-Computational methodology

Quantum chemical calculations were facilitated by Gaussian '09 computational platform where the modelled and optimized structures were visualized with the aid of Gauss View interface [6]. The energy and molecular properties including geometric optimization and generation of frontier orbitals were performed using DFT quantum level relying on B3LYP correlation functional and 321-G basis set. Global reactivity descriptors; global hardness (η), global softness (S), electrophilicity index (ω), chemical potential (μ), and the frontier orbitals energy gap (**HOMO – LUMO**) were all computed from the energies of the frontier molecular orbitals following the Parr and Yang, Pearson explanation of the global quantities [7,8]. Moreover, Gaussian computational suite enabled the estimation of the overall enthalpy change for a reaction by first performing thermochemistry calculations [9]. The output from Gaussian computational platform was loaded onto Chemission computational code in order to generate 2-D electron density maps.

2- Results and Discussion

In this work, we propose that monomeric cellulose thermally fragments through a series of reaction steps to yield acrolein. Acrolein further fragments by loss of carbon monoxide to form ethene which subsequently forms vinyl free radical via hydrogen radical abstraction in agreement with the previous studies reported in literature [10]. In this study, we have proposed an alternative pathway for the formation of the vinyl radical from acrolein which on the basis of the low energy barrier is remarkably feasible. Tyrosine, on the other hand, degrades as proposed in to form phenol among the other degradants such as cresols. Phenol is of interest in this work because it combines with the vinyl radical to form benzofuran, and subsequently 7-methylbenzofuran and 2-methylbenzofuran via

successive reactions involving the abstraction of hydrogen radical and addition of methyl radicals.

2-1-The proposed mechanistic pathway for phenol and cresol formation

Independent thermal degradation of cellulose and characterization of respective molecular products is not the centerpiece of this study because several studies have investigated the individual pyrolysis of cellulose and tyrosine [11,12]. A few studies have also explored the thermal degradation patterns of some amino acids and lignocellulosic materials in processes such as high temperature cooking and biofuel production [13,14]. Thermally induced fragmentation of aromatic amino acids has been known to yield phenol and alkyl phenols [15,16]. This observation is also in agreement with the other findings on the co-pyrolysis of lignocellulosic biomass and amino acids [15]. The study further reported that only lignin among the lignocellulose biomass yielded phenols whereas amino acids (N-species) yielded a higher quantity of phenols and cresols and no phenols are produced from cellulose pyrolysis. As mentioned elsewhere in literature, phenol is initially isolated in significant amounts from the pyrolysis of the binary mixture of cellulose and tyrosine at ≈ 400 °C [1]. Tyrosine in this case is the precursor for the formation of phenol, cresols, and p-ethyl phenol [14].

At higher pyrolysis temperature of 500 °C, the yield of benzofuran from heat induced decomposition of model biomass materials such as cellulose and tyrosine mixture is noted to achieve a maximum. Generally, benzofuran is the major furan-based compound between 300 and 500 °C, although, 2-methylbenzofuran and 7-methylbenzofuran have been known to form in significant amounts in this temperature range [1]. Various mechanistic channels for furans' formation have been explored in literature with precursors such as sugars, amino acids, and ascorbic acid [17,18]. Some studies have described the factors influencing furan formation

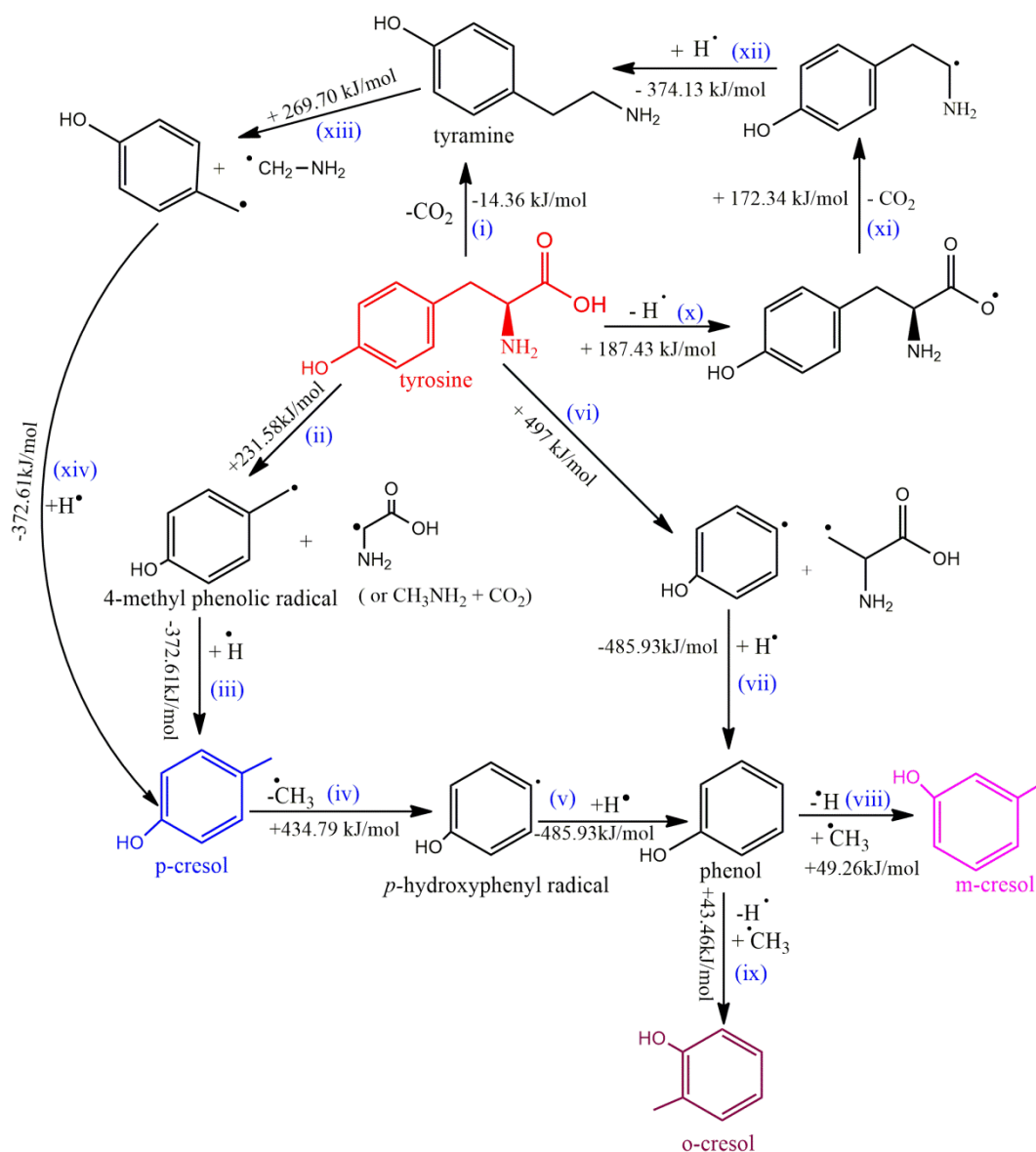
from sugars and amino acids [19], but there is limited information on the influence of amino acids on furan formation from the thermal degradation of lignocellulosic-amino acid mixture. Majority of the pyrolytic processes of these materials gave hypothetical illustrations on the formation of furans by Maillard and Strecker reactions [18,20,21].

The mechanistic formation of molecular species from the pyrolytic decomposition of organic matter composed of N-biomass is not clearly understood. However, certain assumptions on the interaction behavior of the model biomass materials are necessary. Quantitative yields of molecular products depend on the pyrolysis temperature and the residence time. The description of thermal degradation behaviour of amino acids is yet to be understood [22].

In this work, we propose that tyrosine undergoes thermal fragmentation via two competing facile decarboxylation pathways (i) and (ii) as presented in Scheme 1. The first decarboxylation reaction proceeds via the step designated (i) to yield tyramine which involves an exothermic process of -14.36 kJ/mol. The second decarboxylation reaction designated in Scheme 1 as (ii) occurs via the rupture of the C-C bond of the carbon chain by β -fission, a process proceeding by the absorption a heat change of 231.58 kJ/mol to form 4-methylbenzyl radical. Nonetheless, deamination and dehydration reactions cannot be ruled out [10].

In this work, we disregarded α -fission because of its apparent inability to yield phenol and cresols. Initially, β -fission yields 4-methylphenoxy radical which subsequently transforms to *p*-cresol through step (iii). This reaction proceeds via an enthalpy change of 372.61 kJ/mol. On the hand, *p*-cresol undergoes C-C rapture as shown in step (iv) by an absorption of 434.79 kJ/mol of energy to form *p*-hydroxyphenyl radical which in turn undergoes radical-radical interaction with hydrogen radical via step (v) to yield phenol accompanied by the evolution of - 485.93 kJ/mol.

The formation of phenol from *p*-cresol by inductive and mesomeric effects has also been reported in literature [23]. The other cresols such as *o*-cresol and *m*-cresol are formed from phenol by the abstraction of hydrogen radical and subsequent addition of methyl radicals as illustrated in steps (viii) and (ix) which occur via enthalpy changes of 49.26 kJ/mol and 43.46 kJ/mol, respectively. Moreover, tyrosine undergoes hydrogen radical abstraction in step (x) accompanied by the absorption of heat (187.43 kJ/mol) resulting in the formation of tyrosyl radical. Tyrosyl radical transforms into tyraminyl radical via step (xi). This step occurs with the absorption of heat of 172.34 kJ/mol. Tyraminyl radical abstracts a hydrogen radical via step (xii) to form tyramine. Tyramine, on the other hand, undergoes deamination to form 4-methyl phenolic radical via step (xiii). Remarkably, steps (xiv) and (iii) proceed with the addition of hydrogen radical to form *p*-cresol accompanied by evolution similar heat energy of -372.61 kJ/mol. It is important to note that steps (ii) and (vi) proceed to form resonance structures. Therefore, their net enthalpy changes are related to the stability of a resonance structures resulting from these pathways. With less positive or more negative an enthalpy change, the stable the resonance structures are enhanced [24]. The pathway leading to step (ii) is less endothermic when compared with step (vi). This is attributable to the formation of comparatively more stable resonance hybrid structures formed from step (ii). Furthermore, 4-methyl phenolic radical is thus more resonance stabilized than *p*-hydroxyphenyl radical owing to charge delocalization. The interaction of amino acids with cellulosic biomass under thermal conditions is a complicated reaction which is yet to be understood [25]. Nonetheless, we propose a mechanistic channel based on the recombination of the thermal fragments of monomeric cellulose and tyrosine to yield important molecular species.



Scheme 1. The proposed mechanistic pathways for the formation of phenol and cresols from tyrosine.

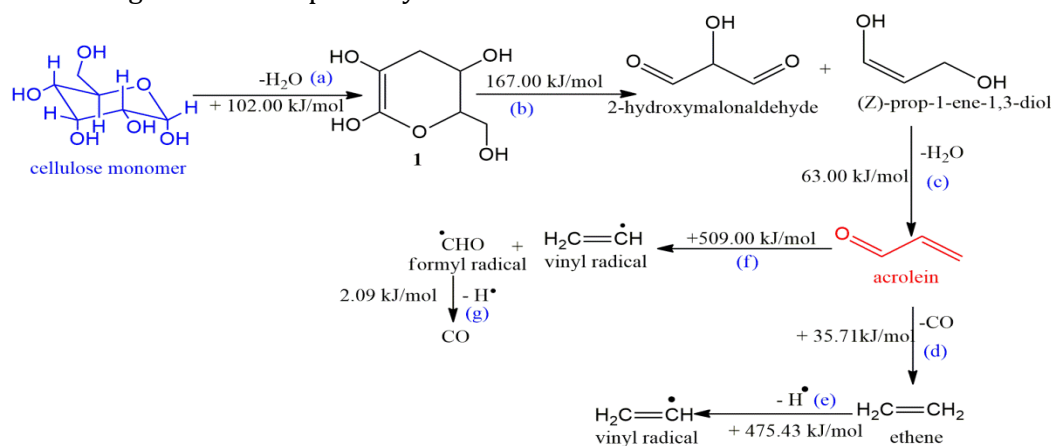
In this work, we disregarded α -fission because of its apparent inability to yield phenol and cresols. Initially, β -fission yields 4-methylphenoxy radical which subsequently transforms to p-cresol through step (iii). This reaction proceeds via an enthalpy change of 372.61 kJ/mol. On the hand, p-cresol undergoes C-C rapture as shown in step (iv) by an absorption of 434.79 kJ/mol of energy to form p-hydroxyphenyl radical which in turn undergoes radical-radical interaction with

hydrogen radical via step (v) to yield phenol accompanied by the evolution of - 485.93 kJ/mol. The formation of phenol from p-cresol by inductive and mesomeric effects has also been reported in literature [23]. The other cresols such as o-cresol and m-cresol are formed from phenol by the abstraction of hydrogen radical and subsequent addition of methyl radicals as illustrated in steps (viii) and (ix) which occur via enthalpy changes of 49.26 kJ/mol and 43.46

kJ/mol, respectively. Moreover, tyrosine undergoes hydrogen radical abstraction in step (x) accompanied by the absorption of heat (187.43 kJ/mol) resulting in the formation of tyrosyl radical. Tyrosyl radical transforms into tyraminyl radical via step (xi). This step occurs with the absorption of heat of 172.34 kJ/mol. Tyraminyl radical abstracts a hydrogen radical via step (xii) to form tyramine. Tyramine, on the other hand, undergoes deamination to form 4-methyl phenolic radical via step (xiii). Remarkably, steps (xiv) and (iii) proceed with the addition of hydrogen radical to form *p*-cresol accompanied by evolution similar heat energy of -372.61 kJ/mol. It is important to note that steps (ii) and (vi) proceed to form resonance structures. Therefore, their net enthalpy changes are related to the stability of a resonance structures resulting from these pathways. With

less positive or more negative an enthalpy change, the stable the resonance structures are enhanced [24]. The pathway leading to step (ii) is less endothermic when compared with step (vi). This is attributable to the formation of comparatively more stable resonance hybrid structures formed from step (ii). Furthermore, 4-methyl phenolic radical is thus more resonance stabilized than *p*-hydroxyphenyl radical owing to charge delocalization.

The interaction of amino acids with cellulosic biomass under thermal conditions is a complicated reaction which is yet to be understood [25]. Nonetheless, we propose a mechanistic channel based on the recombination of the thermal fragments of monomeric cellulose and tyrosine to yield important molecular species.

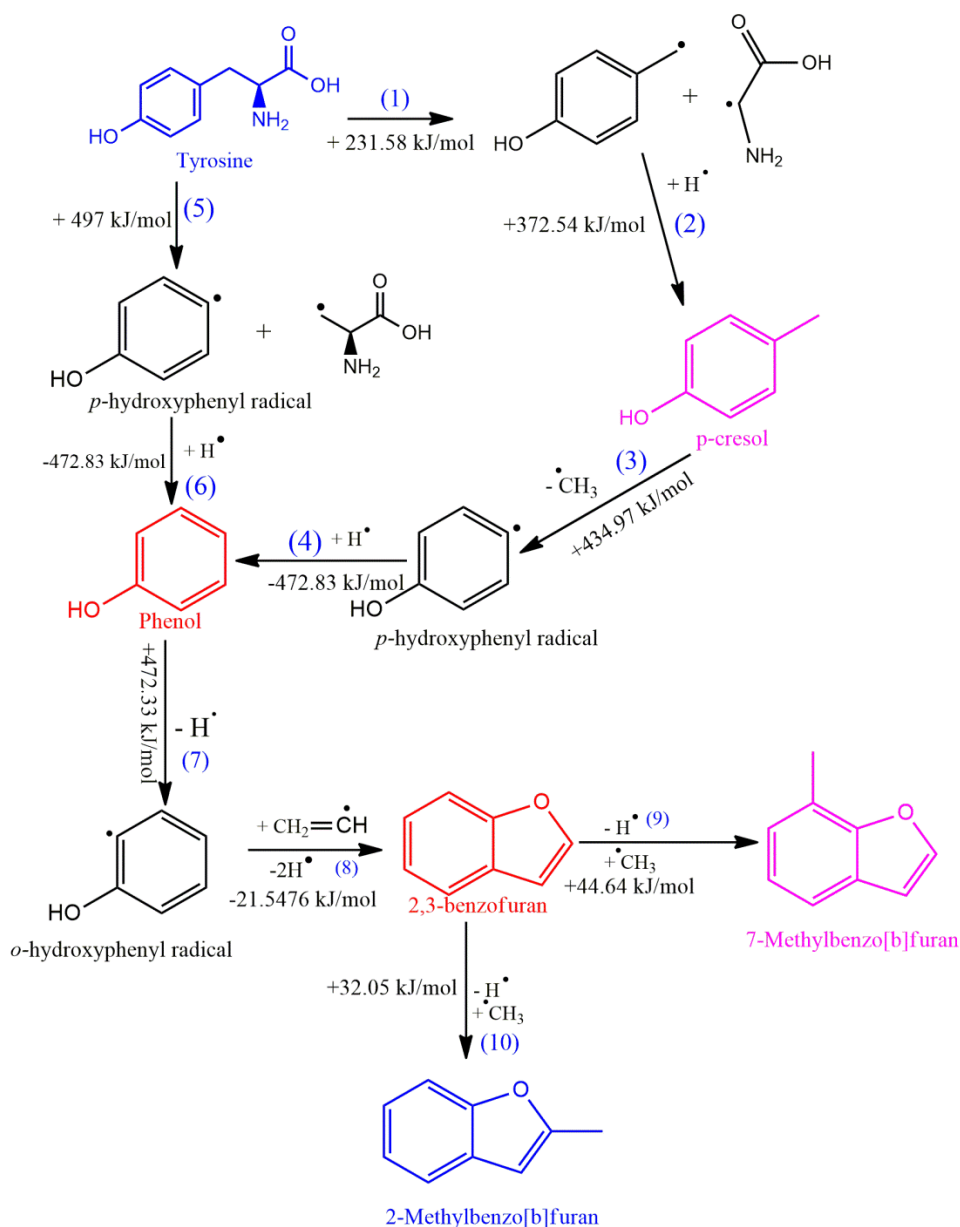


Scheme 2. The proposed mechanism for the degradation of monomeric cellulose to acrolein, ethene and vinyl radical.

The decomposition of cellulose monomer to acrolein has been described elsewhere in the literature [26]. This mechanism has been modified in this study by incorporating the work of Castro and Rust [27]. Herein, we propose that acrolein fragments under pyrolytic conditions form ethene and subsequently vinyl radical as illustrated in Scheme 2. Furthermore, we propose that vinyl radical and phenol are the key precursors for the formation of benzofurans.

2-2- The proposed mechanism for the formation of furans

Among the other possible mechanistic channels, and as reported in Scheme 3, phenol combines with vinyl radical to form the principal product, benzofuran. Two feasible pathways for the fragmentation of tyrosine to form phenol i.e. steps 1 and 5, are proposed.



Scheme 3. The proposed mechanistic pathway for the formation of benzofuran and its methylated analogues.

Step 5 is the concerted rapturing of the C–C bond in tyrosine to form *p*-hydroxyphenyl radical accompanied by an enthalpy change of 497 kJ/mol [28]. Step 6 indicates the formation of a C–H bond in which *p*-hydroxyphenyl radical abstracts a hydrogen radical to form phenol proceeding with the release of 472.83 kJ/mol. The abstraction of hydrogen radical from phenol as shown in step 7 to form *o*-hydroxyphenyl

radical ultimately leads to the formation of phenol resulting in an enthalpy change of 472.33 kJ/mol. In the benzofuran formation, *o*-hydroxyphenyl radical is proposed to combine with vinyl radical. This step proceeds with the removal of two hydrogen radicals. Concerning an enthalpy change of -21.55 kJ/mol, this route is feasible (step 8). The abstraction of a hydrogen radical (steps 9 and 10) followed by addition of a

methyl radical results in the formation of 7-methylbenzofuran and 2-methylbenzofuran, respectively, accompanied enthalpy changes of 44.64 kJ/mol and 32.05 kJ/mol, respectively.

2-3-Frontier molecular orbitals

The highest occupied molecular orbital (HOMO) and the lowest unoccupied molecular orbital (LUMO) are defined as frontier molecular orbitals [29] and they determine how molecules interact [29,30]. Generally, the HOMO of a molecule interacts by overlapping with the LUMO of another molecule in a given chemical reaction [30]. Typically, the HOMO is regarded as the nucleophile, and therefore the electron donor. Its energy (ϵ_{HOMO}) equals the electron affinity (EA). On the other hand, the LUMO is considered as the electrophilic site, and thus the electron accepting orbital with its energy (ϵ_{LUMO}) being typically related to the ionization potential (IP) [31]. One of the most significant features of the frontier orbitals is the frontier orbitals gap (HOMO – LUMO) gap, which is useful in determining the chemical reactivity and the kinetic stability of an organic molecule. A molecule with a small HOMO – LUMO energy gap has a high reactivity, but low kinetic stability [32]. That is, molecules with high HOMO – LUMO energy gap are generally stable, less polarized, and thus chemically inert. Conversely, a molecule with a small frontier orbital energy gap is more polarized and is designated as soft [33]. The increased chemical reactivity owing to the smaller energy gap can be explained based on the fact that addition of electrons to a high-lying LUMO is energetically favored. The electrons removal from a low-lying HOMO in a given reaction is equally energetically preferred [34]. The computational studies have focused on the possibility of using frontier orbital energy gaps in determining molecular electrical transport properties and charge transfer interactions [30].

2-4-Global reactivity parameters

The global hardness (η), global softness (S), chemical potential (μ), electrophilicity index (ω), and electronegativity (χ) are the global reactivity descriptors that characterize the behaviour of atoms and molecules [35], and are regarded as chemical reactivity predictors [31]. The global electrophilicity (ω) was initially determined by Parr *et al.* [30] and is described as the change in energy occasioned by transition of electrons from the HOMO to the LUMO levels [32]. This quantity predicts the chemical reactivity and electrophilic character of molecules [30]. Electrophilicity index is directly correlated to electrophilic character [36]. The global electrophilicity quantity is defined as expressed in Equation 5.

$$\omega = \frac{\mu^2}{2\eta} \quad (5)$$

Where, μ represents the chemical potential and η is the global hardness.

The global hardness initially introduced by Pearson (1986) describes the overall stability of a system [37]. This quantity was determined using Equation 6.

$$\text{Global hardness } (\eta) = \frac{\epsilon_{LUMO} - \epsilon_{HOMO}}{2} \quad (6)$$

The global softness designated as S, is by definition, the inverse of global hardness and is computed using Equation 7.

$$S = \frac{1}{\eta} \quad (7)$$

This equation was utilized to determine the softness of the molecular products examined in this study. Evidently from Table 1, the molecule with the greatest global hardness has lower global softness, implying greater chemical inertness. For instance, p-cresol (1.72 eV) has a lower hardness compared with phenol (2.163 eV), implying a higher reactivity of p-cresol. This comparison is in agreement with the reactivity order based on the HOMO – LUMO energy gap discussed earlier in this work as well as in the other previous studies [30,32]. 7-

methylbenzofuran has lower hardness, and thus greater softness compared to 7-methylbenzofuran with a global hardness of 1.633 eV. The global hardness for benzofuran and 7-methylbenzo[b]furan is 2.028 eV and 1.728 eV, respectively. Thus, benzofuran is the hardest and thus has the greatest chemical stability.

From the density functional theory formalism, the chemical potential μ is regarded as the Lagrange multiplier in the Euler-Lagrange equation [8]. The electronegativity (χ) which is a measure of tendency of an atom to attract electrons has been established to be the negative of the chemical potential, μ [38] and is expressed by equation 8.

$$\mu = \left(\frac{\partial E}{\partial N} \right)_{v(r)} = -\chi \quad (8)$$

The chemical potential (μ) can conveniently be obtained from the frontier molecular orbitals in the ground state, as shown in Equation 9 [30].

$$(\mu) = \frac{\epsilon_{\text{LUMO}} + \epsilon_{\text{HOMO}}}{2} = -\chi \quad (9)$$

2-5-Electron density maps

In this study, the **HOMO – LUMO** energy gap was determined for the molecular products phenol, p-cresol, and benzofuran. These compounds were modelled, and the frontier orbitals **HOMO – LUMO** energy gaps were determined for the optimized structures reported in Figure 1. DFT allows for determining the electron density maps of the optimized molecular structures [35]. In this work, electron potentials were displayed on the total electron density surface. Electron density map (EDM) reveals electron distributions in a molecule as a consequence of bond formation [39], and it is very important when describing bond interactions [40].

The electron cloud is larger where there are more electrons, and the colour spectrum describes variation in the electron density, often, the change in the electron density map colour

from blue to red, representing increasing electron density. The **HOMO – LUMO** molecular orbitals and the optimized geometrical structures of selected molecular species of interest are given in Figure 1. The red colour in the electron density map is associated with a negative potential and represents the site for electrophilic attack. The colour intensity is of significance, for instance, the deep red color in a region between two covalently bonded atoms indicates greater overlap of the electron cloud and stronger covalent interaction [41]. The blue colour shows the highest electrostatic potential energy which happens when the excited state density is greater than the ground state density [42]. This region, together with the green area, has positive potential, and is therefore a good center for nucleophilic attack. It is evident from the electron density maps and electron potential surfaces that phenol, benzofuran, and 2-methylbenzofuran have greater electron cloud overlap and covalent interactions are greater around the aromatic ring as can be observed from the intensity of their electron distribution.

The values in Table 1 clearly present that p-cresol had a smaller energy difference of 3.456 eV compared with phenol whose frontier orbital energy gap is 4.327 eV, and thus p-cresol is more reactive notwithstanding its lower kinetic stability. Alkylated benzofurans are more reactive than benzofuran because of their lower **HOMO – LUMO** energy gaps. On the other hand, 2-methylbenzo[b]furan has an energy gap of 3.265 eV. This value is relatively lower than that of 7-methylbenzo[b]furan whose computed energy difference is 3.456 eV, and thus 2-methylbenzo[b]furan is more reactive compared with 7-methylbenzo[b]furan.

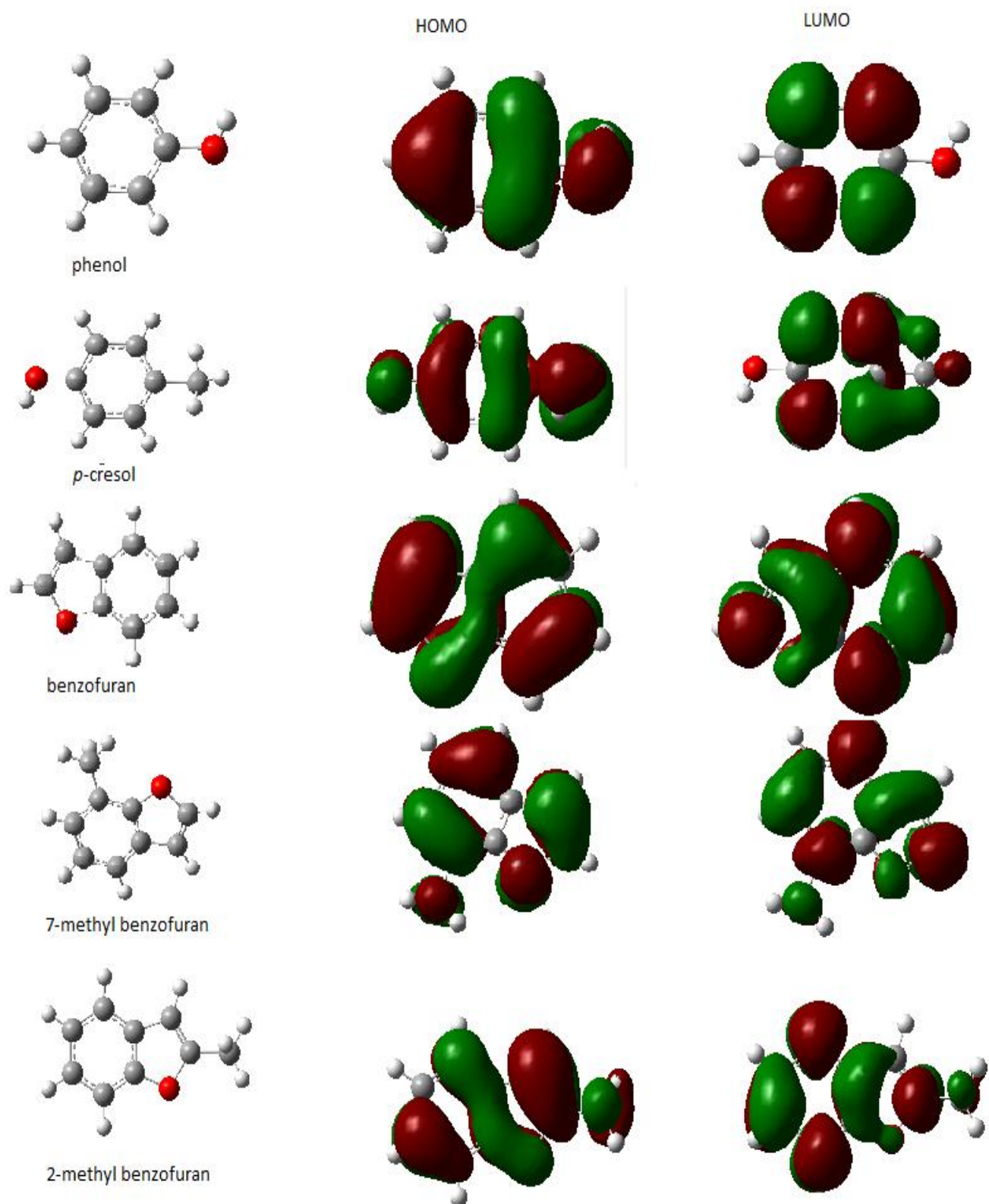


Fig. 1. The optimized geometrical structures and molecular orbitals of selected molecular products.

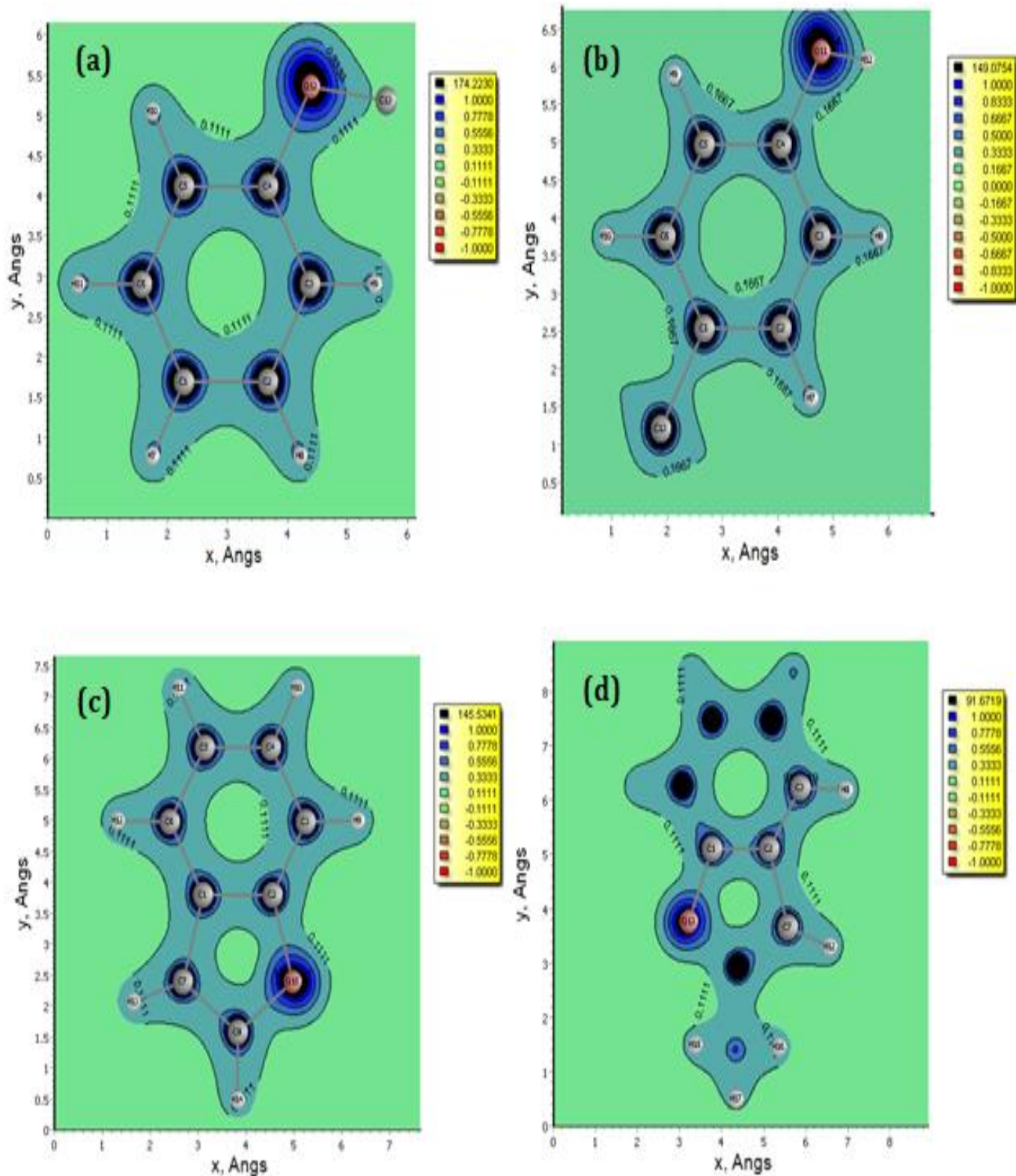


Fig. 2. Electron density maps displaying electrostatic potentials and electron density surfaces for (a) phenol (b) p-cresol (c) benzofuran and (d) 2-methylbenzofuran.

Table 1. HOMO-LUMO energy gaps and global reactivity descriptors of selected phenolic and furan-based molecular products

Compound	ϵ_{HOMO} (eV)	ϵ_{LUMO} (eV)	$\Delta E = \epsilon_{LUMO} - \epsilon_{HOMO}$ (eV)	$\eta = \frac{\epsilon_{LUMO} - \epsilon_{HOMO}}{2}$ (eV)	$\mu = \frac{1}{\eta}$ (eV)	$\omega = \frac{\epsilon_{LUMO} + \epsilon_{HOMO}}{2}$ (eV)	$\omega^2 = \frac{\mu^2}{2\eta}$ (eV)
Phenol	-9.252	-4.925	4.327	2.163	0.462	-7.089	11.617
p-cresol	-8.463	-5.007	3.456	1.728	0.579	-7.007	14.207
Benzofuran	-9.116	-5.061	4.055	2.028	0.493	-7.089	12.390
2-methylbenzo[b]furan	-8.163	-4.898	3.265	1.633	0.612	-6.531	13.060
7-methylbenzo[b]furan	-8.245	-4.789	3.456	1.728	0.579	-6.517	12.289

Legend: η =Global hardness (eV), S =Global softness (eV), μ =Chemical potential (eV), and ω =Electrophilicity index (eV).

Nevertheless, these energies are significantly close thus the two molecules have comparable excitation energies [43]. Although benzofuran has the lowest reactivity, it has the highest kinetic stability because of the relatively high **HOMO – LUMO** energy gap among the benzofurans. Of the molecular products of interest, p-cresol had the highest electrophilicity index of 14.207 eV and is thus a strong electrophile. Phenol had a ω value of 11.617 eV, which is lower than that of cresol. Therefore, phenol is a weaker electrophile compared with p-cresol. Among the benzofurans, 2-methylbenzo[b]furan had the highest ω of 13.06 eV, and thus it has the highest electrophilicity in the furan category. The other benzofurans have comparable values of ω . For instance; 2-methylbenzo[b]furan had $\omega = 12.029$ eV compared to that of benzofuran whose electrophilicity index was 12.39 eV. The chemical potentials for the molecular products of pyrolysis considered in this study were calculated from the frontier orbitals and reported in Table 1. The chemical potential is invaluable while concerning the reactivity of molecular compounds [32]. Generally, molecules with greater values of μ are more reactive than those with smaller values of μ [30,32]. The DFT derived calculation of μ based on the **HOMO – LUMO** energies were; p-cresol (-7.007 eV), phenol (-7.089 eV), benzofuran (-

7.089 eV), 2-methylbenzo[b]furan (-6.531 eV), and 7-methylbenzo[b]furan (-6.517 eV).

3-Conclusion

This study has proposed an extensive mechanistic description for the formation of phenol, cresols, and selected benzofurans from the thermal treatment of model biomass composition–cellulose and tyrosine. Therefore, the formation of phenol and cresols cannot be objectively attributed to the thermal degradation of cellulose at least from a mechanistic standpoint. It is suggested that phenol is formed from thermal fragmentation of tyrosine through C–C scission and free radical interactions. On the other hand, benzofuran and its alkylated versions are proposed to form via radical recombination as reported herein. Monomeric cellulose undergoes fragmentation to yield various intermediates that give lower molecular weight unsaturated molecules such as ethene which is the main precursor for the formation of chemically labile vinyl radical. *o*-hydroxyphenyl radical, a tyrosine degradant combines with the vinyl radical to yield benzofuran. Moreover, the low enthalpy changes reported for decarboxylation and deamination of tyrosine to form various molecular products is in agreement with the previous studies. The global descriptors were computed to understand the electrophilicity, chemical stability, and kinetic

stability of the pyrolysis molecular products. As a result, p-cresol was found to be the most chemically unstable, least kinetically stable, and with the highest electrophilic character. Its derivative; phenol had the highest global hardness, and therefore the most chemically inert and kinetically stable. In the furan family, the alkylated furans were observed to be more reactive than benzofuran.

Declarations

Ethics approval and consent to participate

Not Applicable.

Consent for publication

This article has the consent of all the authors.

Availability of data and materials

The data associated with the findings of this study are available from the corresponding author upon reasonable request.

Competing interests

The authors have no competing interests.

Funding

This study received no specific grants from any funding agency.

References

- [1]. J.K. Kibet, L. Khachatryan, B. Dellinger, Phenols from pyrolysis and co-pyrolysis of tobacco biomass components. *Chemosphere*, 138, (2015) 259-265.
- [2] J.L. Gázquez, Perspectives on the density functional theory of chemical reactivity. *Journal of the Mexican Chemical Society*, 52 (2008) 3-10.
- [3]. L.R. Domingo, P. Pérez, J.A. Sáez. Understanding the local reactivity in polar organic reactions through electrophilic and nucleophilic Parr functions. *RSC advances*, 3(5) (2013) 1486-1494.
- [4]. L.A.Z. Hernández, R.L. Camacho-Mendoza, S. González-Montiel, J. Cruz-Borbolla. The chemical reactivity and QSPR of organic compounds applied to dye-sensitized solar cells using DFT. *Journal of Molecular Graphics and Modelling*, 104 (2021) 107852.
- [5]. P. Fuentealba and C. Cárdenas. Density functional theory of chemical reactivity. In: *Chemical modelling*, (2014) 151-174.
- [6]. M. Frisch, G. Trucks, H. Schlegel, G. Scuseria, M. Robb, J. Cheeseman, G. Scalmani, V. Barone, B. Mennucci and G.A. Petersson; et al. *Gaussian 09, Revision A. 01*; Gaussian. Inc.: Wallingford, CT, (2009)
- [7] R. G. Pearson. The HSAB principle—more quantitative aspects. *Inorganica Chimica Acta*, 240(1-2) (1995) 93-98.
- [8]. W. Yang and R. G. Parr. Hardness, softness, and the Fukui function in the electronic theory of metals and catalysis. *Proceedings of the National Academy of Sciences*, 82(20) (1985) 6723-6726.
- [9]. D. W. Rogers, A. A. Zavitsas and L. K. Rogers-Bennett. The Gaussian G4 structure, enthalpy, and free energy of formation of trans-dimethyl-, diethyl-, dipropyl-, and dibutylcyclopentanes. *Journal of molecular modeling*, 25(8) (2019) 1-7.
- [10]. G. Liu, M. M. Wright, Q. Zhao, R.C. Brown, K. Wang and Y. Xue. Catalytic pyrolysis of amino acids: comparison of aliphatic amino acid and cyclic amino acid. *Energy Conversion and Management*, 112 (2016) 220-225.
- [11]. C. Zhang, L. Chao, Z. Zhang, L. Zhang, Q. Li, H. Fan, S. Zhang, Q. Liu, Y. Qiao and Y. Tian. Pyrolysis of cellulose: Evolution of functionalities and structure of bio-char versus temperature. *Renewable and sustainable energy reviews*, 135 (2021) 110416.
- [12]. N. Hassan, A. Jalil, C. Hitam, D. Vo and W. Nabgan. Biofuels and renewable chemicals production by catalytic pyrolysis of cellulose: a review. *Environmental Chemistry Letters*, 18(5) (2020) 1625-1648.
- [13]. J. Bai, H. Gao, J. Xu, L. Li, P. Zheng, P. Li, J. Song, C. Chang and S. Pang. Comprehensive study on the pyrolysis product

- characteristics of tobacco stems based on a novel nitrogen-enriched pyrolysis method. *Energy*, (2021) 122535-122535.
- [14]. L. Jie, L. Yuwen, S. Jingyan, W. Zhiyong, H. Ling, Y. Xi and W. Cunxin. The investigation of thermal decomposition pathways of phenylalanine and tyrosine by TG-FTIR. *Thermochimica acta*, 467(1-2) (2008) 20-29.
- [15] H. Chen, Y. Xie, W. Chen, M. Xia, K. Li, Z. Chen, Y. Chen, H. Yang. Investigation on co-pyrolysis of lignocellulosic biomass and amino acids using TG-FTIR and Py-GC/MS. *Energy Conversion and Management*, 196 (2019) 320-329.
- [16]. R.K. Sharma, W.G. Chan, J.I. Seeman and M.R. Hajaligol. Formation of low molecular weight heterocycles and polycyclic aromatic compounds (PACs) in the pyrolysis of α -amino acids. *Journal of Analytical and Applied Pyrolysis*, 66(1-2) (2003) 97-121.
- [17]. C. Perez Locas, V.A. Yaylayan. Origin and mechanistic pathways of formation of the parent furan A food toxicant. *Journal of Agricultural and Food Chemistry*, 52(22) (2004) 6830-6836.
- [18]. F. Van Lancker, A. Adams, A. Owczarek-Fendor, B. De Meulenaer and N. De Kimpe. Mechanistic Insights into Furan Formation in Maillard Model Systems. *Journal of Agricultural and Food Chemistry*, 59(1) (2011) 229-235.
- [19]. S. Nie, J. Huang, J. Hu, Y. Zhang, S. Wang, C. Li, M. Marcone and M. Xie. Effect of pH, temperature and heating time on the formation of furan in sugar-glycine model systems. *Food Science and Human Wellness*, 2(2) (2013) 87-92.
- [20]. Y.J. Seok, J.Y. Her, Y.G. Kim, Y.M. Kim, S.Y. Jeong, M.K. Kim, J.Y. Lee, C.I. Kim, H.J. Yoon and K.G. Lee. Furan in thermally processed foods-a review. *Toxicological Research*, 31(3) (2015) 241-253.
- [21]. A. Adams, F. Van Lancker, A. Owczarek-Fendor, B. De Meulenaer and N. De Kimpe. Mechanistic insights into furan formation in Maillard model systems. *Journal of Agricultural and Food Chemistry*, 59(1) (2011) 229-235.
- [22]. D. Jiang, J. Li, S. Wang, H. Li, L. Qian, B. Li, X. Cheng, Y. Hu and X. Hu. Cyclic compound formation mechanisms during pyrolysis of typical aliphatic acidic amino acids. *ACS Sustainable Chemistry & Engineering*, 8(45) (2020) 16968-16978.
- [23]. S.C. Moldoveanu. Pyrolysis of organic molecules. In: *Pyrolysis of Other Nitrogen-Containing Compounds*, Elsevier, (2019).
- [24]. T. Sugahara, D. Hashizume, N. Tokitoh, H. Matsui, R. Kishi, M. Nakano and T. Sasamori. Characterization of resonance structures in aromatic rings of benzene and its heavier-element analogues. *Physical Chemistry Chemical Physics*, 24(37) (2022) 22557-22561.
- [25]. P. Zong, Y. Jiang, Y. Tian, J. Li, M. Yuan, Y. Ji, M. Chen, D. Li and Y. Qiao. Pyrolysis behavior and product distributions of biomass six group components: Starch, cellulose, hemicellulose, lignin, protein and oil. *Energy Conversion and Management*, 216, (2020) 112777.
- [26]. P. Humphreys, A. Laws and J. Dawson. A review of cellulose degradation and the fate of degradation products under repository conditions, (2010).
- [27]. C. Castro and F. Rust. Thermal decomposition of acrolein. The attack of methyl and t-butoxy free radicals on acrolein. *Journal of the American Chemical Society*, 83(24) (1961) 4928-4932.
- [28]. J. Zhang, Z. Shao, Y. Hu, B. Liu, Y. Zhang and S. Wang. Formation of a creatinine thermal degradation product and its role and participation in the radical pathway of forming the pyridine ring of 2-amino-1-methyl-6-phenylimidazo [4, 5-b] pyridine (PhIP). *Food chemistry*, 312 (2020) 126083.

- [29]. J. Martínez. Local reactivity descriptors from degenerate frontier molecular orbitals. *Chemical Physics Letters*, 478(4-6) (2009) 310-322.
- [30]. A. Bendjeddou, T. Abbaz, A. Gouasmia and D. Villemin. Molecular structure, HOMO-LUMO, MEP and Fukui function analysis of some TTF-donor substituted molecules using DFT (B3LYP) calculations. *International Research Journal of Pure and Applied Chemistry*, 12(1) (2016) 1-9.
- [31]. F. Pereira, K. Xiao, D.A. Latino, C. Wu, Q. Zhang and J. Aires-de-Sousa. Machine learning methods to predict density functional theory B3LYP energies of HOMO and LUMO orbitals. *Journal of chemical information and modeling*, 57(1) (2017) 11-21.
- [32]. M. Miar, A. Shiroudi, K. Pourshamsian, A. R. Oliaey and F. Hatamjafari. Theoretical investigations on the HOMO-LUMO gap and global reactivity descriptor studies, natural bond orbital, and nucleus-independent chemical shifts analyses of 3-phenylbenzo [d] thiazole-2 (3 H)-imine and its para-substituted derivatives: Solvent and substituent effects. *Journal of Chemical Research*, 45(1-2) (2021) 147-158.
- [33]. A.Q. Nguyen, N.T. Anh, T.A. Nguyễn. *Frontier orbitals: a practical manual*. John Wiley & Sons. (2007)
- [34]. M.J. Hoque, A. Ahsan, M.B. Hossain. Molecular Docking, Pharmacokinetic, and DFT Calculation of Naproxen and its Degradants. *Biomedical Journal of Scientific & Technical Research*, 9(5) (2018) 7360-7365.
- [35] L.R. Domingo, M. Ríos-Gutiérrez, P. Pérez. Applications of the conceptual density functional theory indices to organic chemistry reactivity. *Molecules*, 21(6) (2016) 748.
- [36]. R.G. Parr, L.V. Szentpály, S. Liu. Electrophilicity index. *Journal of the American Chemical Society*, 121(9) (1999) 1922-1924.
- [37]. R.G. Pearson. Absolute electronegativity and hardness correlated with molecular orbital theory. *Proceedings of the National Academy of Sciences*, 83(22) (1986) 8440-8441.
- [38]. K. Chandrakumar and S. Pal. The concept of density functional theory based descriptors and its relation with the reactivity of molecular systems: A semi-quantitative study. *International Journal of Molecular Sciences*, 3(4) (2002) 324-337.
- [39]. L.R. Domingo. Molecular electron density theory: a modern view of reactivity in organic chemistry. *Molecules*, 21(10) (2016) 1319.
- [40]. H. Kasai, K. Tolborg, M. Sist, J. Zhang, V. R. Hathwar, M. Ø. Filsø, S. Cenedese, K. Sugimoto, J. Overgaard and E. Nishibori. X-ray electron density investigation of chemical bonding in van der Waals materials. *Nature materials*, 17(3) (2018) 249-252.
- [41]. J. Chen, Z. Xu, and Y. Chen. *Electronic Structure and Surfaces of Sulfide Minerals: Density Functional Theory and Applications*. Elsevier, (2020).
- [42]. C. Matta and R. Gillespie. Understanding and interpreting molecular electron density distributions. *Journal of Chemical Education*, 79(9) (2002) 1141.
- [43]. T. Stein, J. Autschbach, N. Govind, L. Kronik, R. Baer. Curvature and frontier orbital energies in density functional theory. *The Journal of Physical Chemistry Letters*, 3(24) (2012) 3740-3744.

HOW TO CITE THIS ARTICLE

Samuel K. Kirkok, Joshua K. Kibet, Thomas K. Kinyanjui, Francis I. Okanga. Mechanistic Formation of Phenolic and Based Molecular Products from Pyrolysis of Model Biomass Components. *Prog. Chem. Biochem. Res*, 5(4) (2022) 376-390.

DOI: 10.22034/pcbr.2022.367054.1235

URL: http://www.pcbiochemres.com/article_163466.html

